EUROPEAN ORGANIZATION FOR NUCLEAR RESEARCH

Ref. # 629
July 19, 1997
Parallel sessions: 4
Plenary sessions: 2, 4

QCD studies with e^+e^- annihilation data from 130 to 172 GeV

The ALEPH Collaboration

Abstract

Hadronic events produced at LEP at centre-of-mass energies of 130, 136, 161 and 172 GeV have been studied and compared with QCD predictions. Distributions of event-shape observables, jet rates, momentum spectra and multiplicities are presented and compared to the predictions of several Monte Carlo models and analytic QCD calculations. From a fit of $\mathcal{O}(\alpha_s^2)$+NLLA QCD calculations to the differential two-jet rate, α_s has been determined at various energies. The mean charged particle multiplicities and the peak positions ξ^* in the $\xi = \ln(1/x_p)$ distribution have also been determined. These results have been compared to lower energy data and to analytic QCD or Monte Carlo predictions for their energy evolution.

(Submitted to the 1997 EPS-HEP conference, Jerusalem)

1 Introduction

In the summer of 1996, the centre-of-mass energy of the LEP e^+e^- ring was increased first to 161 and then 172 GeV. In this paper preliminary analyses of hadronic events collected by the ALEPH detector at these energies are presented. The measurements are based on integrated luminosities of 11.1 and 10.6 pb^{-1} at 161 and 172 GeV, respectively. In addition, analyses of hadronic events at 130 and 136 GeV, based on approximately 2.9 pb^{-1} at each energy and published in [1], are updated and extended. The data samples at 130 and 136 GeV are combined, and the resulting corrected distributions correspond to $E_{\rm cm} = 133$ GeV.

The general ideas remain essentially those of [1]. The primary goal is to investigate quantities for which the centre-of-mass energy dependence is well predicted by QCD. By comparing with corresponding measurements based on the data collected at $E_{\rm cm} = M_{\rm Z}$ and also at lower energies, the predictions can be tested. An additional goal of the measurements is to provide a check of QCD-based Monte Carlo models; these are used for estimating backgrounds and efficiencies in many other analyses such as in searches for new particles and in studies of the W boson.

The observables include inclusive charged particle distributions, jet rates, and distributions of event-shape variables. These are compared to QCD predictions, either from QCD-based models or analytic QCD formulae. In addition, a number of quantities are measured such as the mean multiplicity of charged particles, mean values of event-shape variables, and the strong coupling constant α_s. The energy dependence of these quantities is investigated by comparing with corresponding measurements at lower $E_{\rm cm}$.

In Section 2, the event selection and correction procedures are discussed. Results on inclusive and event-shape distributions are shown in Sections 3 and 4. In Section 5, jet rates are presented, and in Section 6, α_s is measured using the distribution of the variable y_3.

2 Experimental procedure

A detailed description of the ALEPH detector is given in [3]. The measurements presented here are based on both charged particle measurements from the time projection chamber, inner tracking chamber, and vertex detector, as well as information on neutral particles from the electromagnetic and hadronic calorimeters. An energy-flow reconstruction algorithm is applied, which takes advantage of the redundancy of energy and momentum measurements and exploits photon, electron and muon identification [4]. The output of this algorithm is a list of "energy-flow objects," with measured momentum vectors and information on particle type.

At centre-of-mass energies higher than the Z resonance, there is a relatively high probability for initial state photon radiation (ISR), resulting in hadronic systems with an invariant mass $\sqrt{s'} \approx M_{\rm Z}$. These events must be rejected in order to study those for which $\sqrt{s'}$ is close to the centre-of-mass energy. An additional source of background at $\sqrt{s} = 161$ and 172 GeV comes from production four-quark states through WW, ZZ and

$Z\gamma^*$ (four-fermion processes). The WW events typically lead to four well-separated jets, and constitute a potentially important background for studies of multijet final states.

The ISR photon(s) are usually emitted at small angles with respect to the beam line and do not enter the detector. In this case, the invariant mass of the measured particles is significantly less than $E_{\rm cm}$, and there is a net imbalance in the total momentum along the beam line (the z direction). In approximately one quarter of the hadronic events, however, a high energy ISR photon enters the detector. These photons must be identified and the remaining system examined to see if it looks like a hadronic Z decay, in which case the event is rejected.

To separate ISR photons from the hadronic system (some of which of course consists of photons from e.g. π^0 decays), the particles in the event are clustered using the Durham algorithm [2] with a resolution parameter of $y_{\rm cut} = 0.002$. Jets are identified in which the fraction of the jet's energy carried by charged hadrons is less than 10%. From these, the photons and any identified electrons (or positrons) are removed; the latter are often the result of photon conversion in the material before the tracking chambers. From the remaining particles, the invariant mass $M_{\rm vis}$ and the absolute value of the sum of the p_z components are computed. Their difference

$$\Delta = M_{\rm vis} - |\sum p_z| \, ,$$

is found to be an effective test variable for separating radiative from non-radiative events. Non-radiative events are selected by requiring $\Delta \geq 0.75\sqrt{s}$. According to Monte Carlo studies based on the PYTHIA generator version 5.7 [5], less than 1% of the accepted events are radiative, having $\sqrt{s'} < 100$ Gev. The measurements of the various quantities use all reconstructed particles of the accepted events, including those which had previously been removed for purposes of computing Δ.

The events passing the anti-ISR cuts still contain some background from four-fermion processes (WW, ZZ, $Z\gamma^*$). These are rejected by first clustering the particles to exactly four jets with the Durham algorithm. The energies of the jets are then rescaled, keeping their directions constant, such that the total energy of the event is equal to $E_{\rm cm}$ and the total momentum is zero. The quantities

$$d^2 = \min \left[\frac{(m_{ij} - M_W)^2 + (m_{kl} - M_W)^2}{M_W^2} \right] \, ,$$

with $M_W = 80.25$ GeV, and

$$c_{WW} = \cos(\text{smallest interjet angle})$$

are then computed, where for d^2 the minimum value is taken among all possible choices of jet pairings ij and kl. Events are then accepted if $d^2 \geq 0.1$ or $c_{WW} \geq 0.9$. The expected WW production cross sections (assuming $M_W = 80.25$ GeV) obtained from the program KORALW [6] are $\sigma_{WW} = 3.77$ pb at 161 and 12.38 pb at 172 GeV. This corresponds to 5.3 expected WW events at 161 GeV, and 15.0 events at 172 GeV. After all cuts, 182, 140, 292 and 254 events are selected at 130, 136, 161 and 172 GeV, respectively.

Corrections for imperfections of the detector and for the residual effects of ISR are made by means of multiplicative factors, as done in [1]. These factors, which are derived from the Monte Carlo model PYTHIA, are by construction approximately independent of the model used. The systematic uncertainty due to a residual model dependence has been estimated by comparing with the results based on correction factors derived from HERWIG version 5.8d [7].

Additional systematic uncertainties, mainly related to the simulation of the detector, are estimated by varying the cuts applied and repeating the analysis. The most significant contribution comes from the variation of the cut value in Δ by $\pm 5\%$, and to a lesser extent in the amount of charged energy allowed in a 'photonic' jet by the same fraction. The charged-track based quantities also show some sensitivity to the minimum transverse momentum allowed. Variations in the WW cross sections used for background subtraction by $\pm 10\%$ led to negligible uncertainties in the corrected distributions. In the event-shape distributions, the systematic uncertainty estimates in each bin are dominated by the small changes in the selected events and tracks as cuts are varied, and hence are very much limited in statistical precision. For this reason, the estimates for neighbouring bins have been averaged in groups of three.

3 Inclusive charged particle distributions

Charged particle inclusive distributions were measured for the variables $\xi = -\ln x_p$, where $x_p = p/p_{\rm beam}$, the rapidity $y = \frac{1}{2}\ln(E + p_\parallel)/(E - p_\parallel)$ with $p_\parallel$ measured with respect to the thrust axis, and the transverse momentum components in and out of the event plane defined by the thrust and major axes, $p_\perp^{\rm in}$ and $p_\perp^{\rm out}$. The thrust axis used for rapidity and the event plane used for $p_\perp^{\rm in}$ and $p_\perp^{\rm out}$ are determined using both charged and neutral particles. The measurements at 133 GeV represent updates of those published in [1]. The update has been done so as to present a set of distributions at different energies all based on the same event selection and analysis technique; the values and assigned errors are very similar to what was given before.

Corrected inclusive distributions of $p_\perp^{in}$, $p_\perp^{out}$ y, and ξ are shown in Figs. 3 – 3, along with the predictions of the models PYTHIA version 5.7 and HERWIG version 5.8, with initial state radiation turned off. The fragmentation and QCD parameters of the models have been tuned using data from $E_{cm} = 91.2$ GeV [9].

Only minor discrepancies with the model predictions are observed. At 161 GeV, however, a significant excess of particles compared to the model predictions at high $p_\perp^{\rm out}$ and at low rapidity can be seen. This is correlated with a large excess in multijet events seen at this energy (cf. Section 5). At 172 GeV, the data are in excellent agreement with models.

By integrating the rapidity distribution, the mean multiplicity of charged particles can be determined. Results for 133, 161 and 172 GeV are given in Table 3.

The multiplicities measured here are shown in Fig. 4 along with measurements from other experiments at various energies [10], and also with the predictions of the Monte

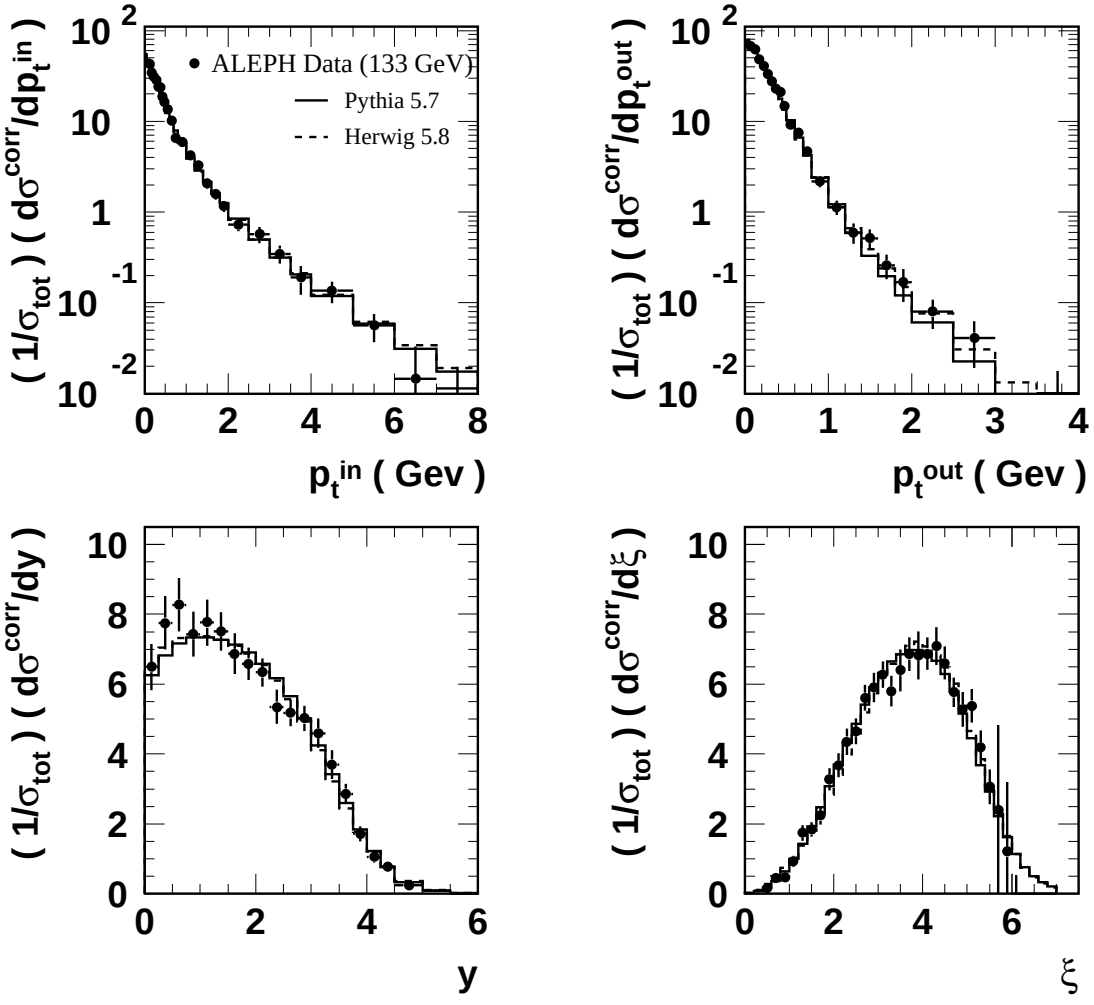

Figure 1: Distributions of $p_\perp^{in}$, $p_\perp^{out}$, rapidity y, and $\xi = -\ln x_p$ at 133 GeV. Statistical and systematic errors are shown added in quadrature.

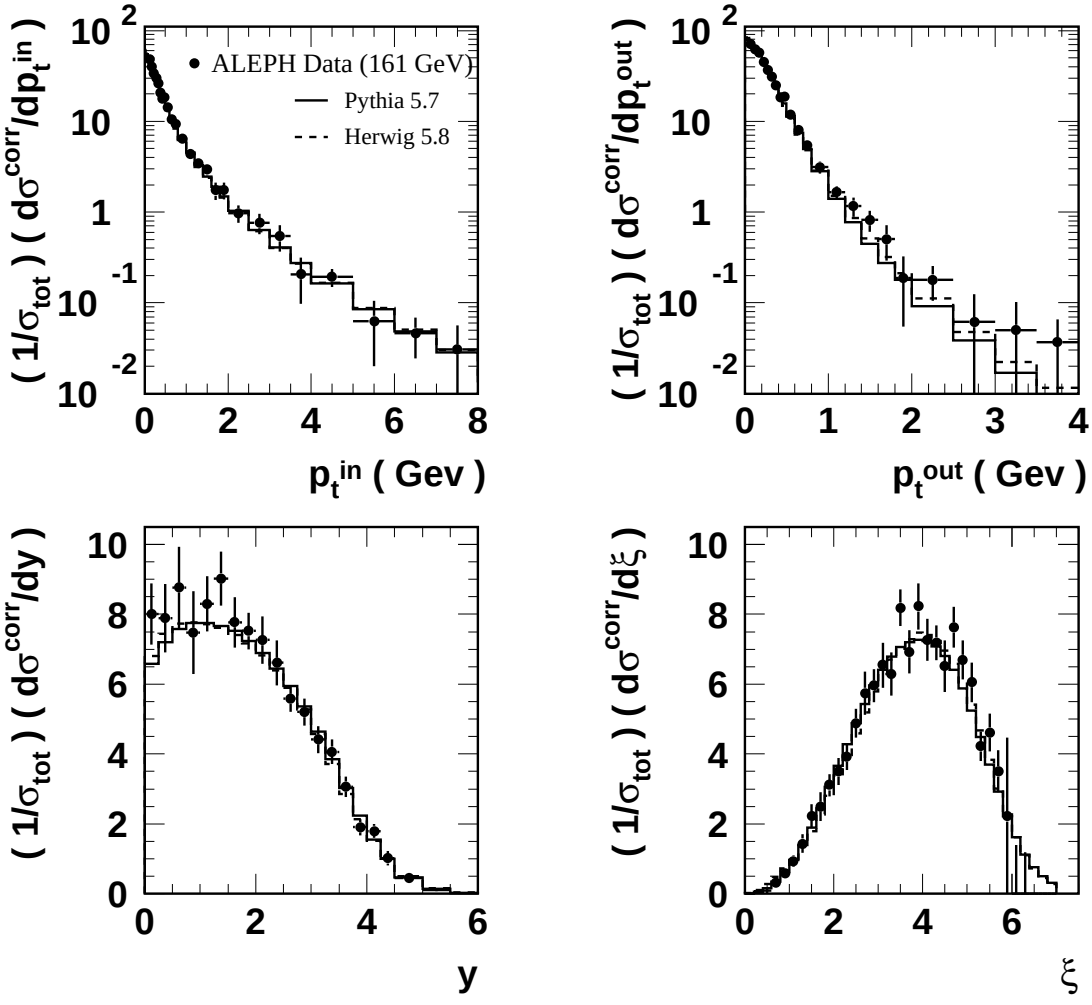

Figure 2: Distributions of $p_\perp^{in}$, $p_\perp^{out}$, rapidity y, and $\xi = -\ln x_p$ at 161 GeV. Statistical and systematic errors are shown added in quadrature.

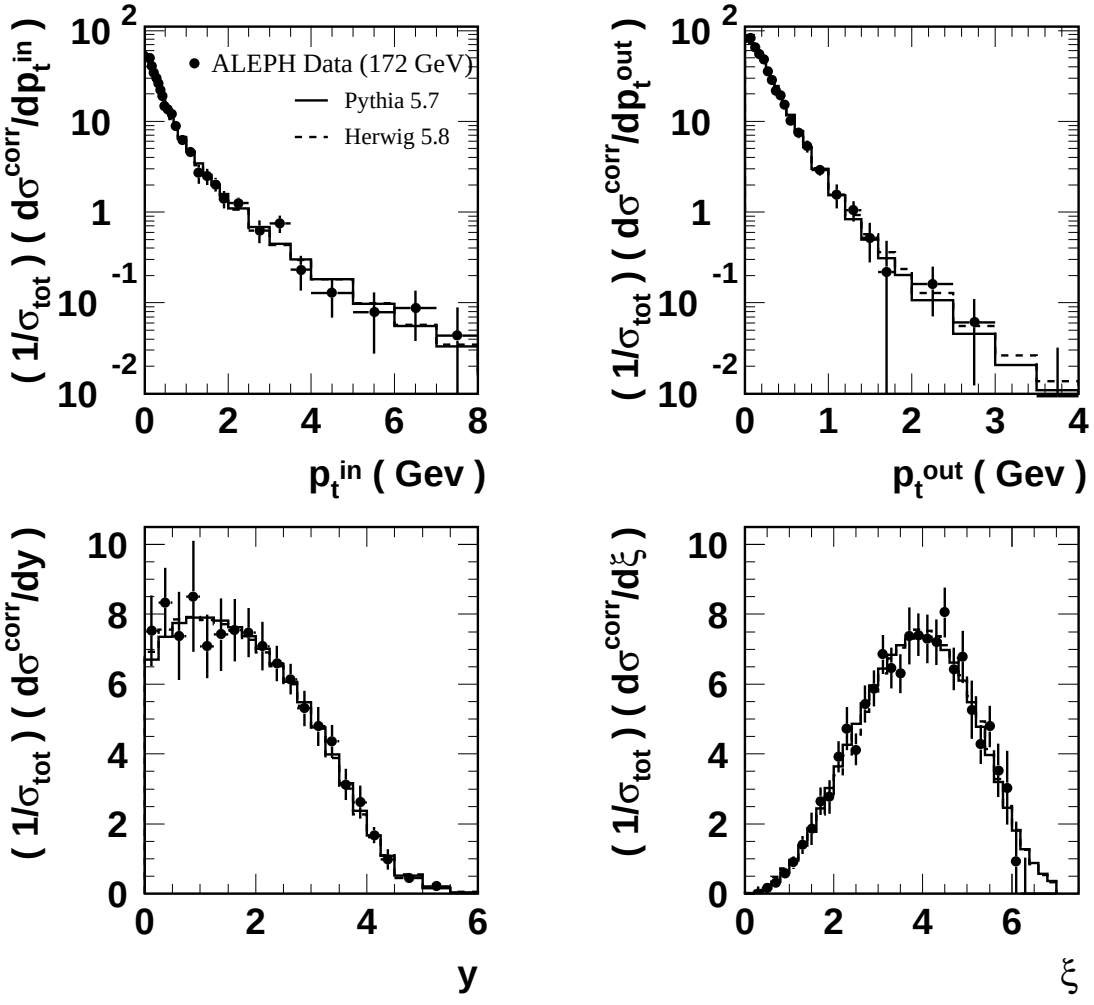

Figure 3: Distributions of $p_\perp^{in}$, $p_\perp^{out}$, rapidity y, and $\xi = -\ln x_p$ at 172 GeV. Statistical and systematic errors are shown added in quadrature.

Table 1: Mean charged particle multiplicity $N_{\rm ch}$ measured at $E_{\rm cm} = 133$, 161 and 172 GeV.

$E_{\rm cm}$ (GeV)	$N_{\rm ch}$	statistical error	systematic error
133	23.99	0.47	0.36
161	26.70	0.58	0.52
172	26.32	0.66	0.53

Carlo models JETSET version 7.4 [5], HERWIG, (both based on parton showers), and also the JETSET model based on the $O(\alpha_s^2)$ matrix element. (Note that for the simulation of hadronic final states in e^+e^- annihilation, JETSET and PYTHIA are essentially equivalent. PYTHIA is used for the detector corrections because of its more accurate description of initial state photon radiation.) The measurement at 161 GeV is somewhat higher than expected from the parton shower based models; this is related to the excess of particles at low rapidity seen in Fig. 3.

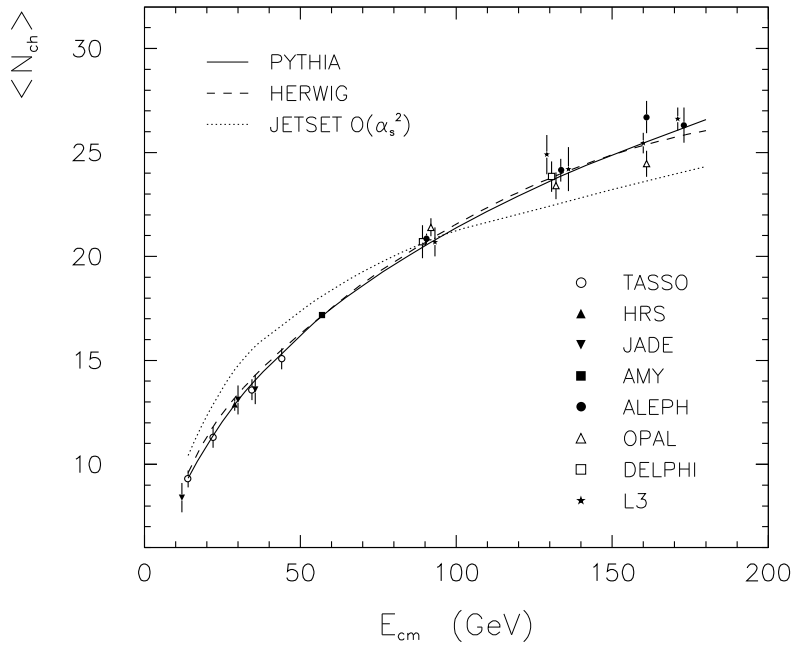

Figure 4: The mean charged particle multiplicity $N_{\rm ch}$ as a function of centre-of-mass energy $E_{\rm cm}$.

As is well known, the matrix element model does not predict a fast enough rise in $N_{\rm ch}$ for increasing energy. Although this model has not been used for LEP I studies as much as those based on parton showers, it is of interest at LEP II, since the $O(\alpha_s^2)$ matrix element is expected to provide a better description of four-jet final states. It is therefore a useful model for predicting backgrounds to WW events. As can be seen from Fig. 4, however, the model parameters need to be retuned at each energy in order to correctly reproduce the mean particle multiplicity.

The peak position ξ^* of the inclusive distribution of ξ was determined by fitting a

distorted Gaussian [11] to the central regions, defined by the width of the distribution at 60% of its maximum height; details of the analysis and error estimation procedure can be found in [1]. The values are given in Table 3 and shown in Figs. 5, along with QCD predictions using the double logarithm approximation (DLA) and including higher order corrections (modified leading logarithm approximation – MLLA) [12]. Also shown in Figs. 5 are the ξ^* values obtained with the same procedure from distributions at lower energies measured by the TASSO experiment [13].

Table 2: The peak position ξ^* of the inclusive charged particle distribution of $\xi = -\ln x_p$, measured at $E_{\rm cm}$ = 133, 161 and 172 GeV. In addition to the errors given, there is a correlated uncertainty due to the choice of fit function of 0.064.

$E_{\rm cm}$ (GeV)	ξ^*	statistical error	systematic error (uncorrelated component)
133	3.968	0.048	0.050
161	4.085	0.071	0.050
172	4.064	0.062	0.071

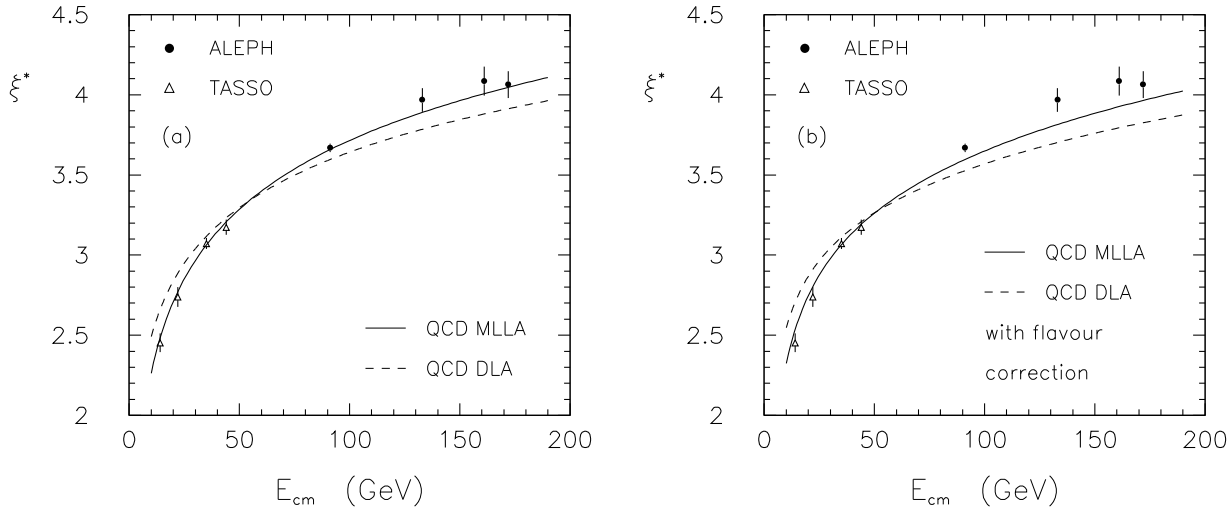

Figure 5: The peak position ξ^* of the distribution of $\xi = -\ln x_p$ as a function of the centre-of-mass energy. In (a) these are compared to the leading order (DLA) and next-to-leading order (MLLA) QCD predictions; in (b) a correction for the energy dependence of the quark flavour mixture is applied (see text). In addition to the error bars shown, there is a correlated uncertainty of 0.064 due to the choice of fit function.

In Fig. 5(a), the predictions are shown without any modification for the effects of hadronisation or the energy dependence of the flavours of primary quarks produced. In Fig. 5(b), a correction for these effects derived from the JETSET model has been applied to the QCD formulae (cf. [9]). As seen in [9], the hadronisation correction leads to somewhat worse agreement with the MLLA curve; this suggests that the excellent agreement

between the data and original MLLA formula could be partially due to a compensation of missing higher order terms by hadronisation and quark mass and flavour effects.

4 Event shapes

The various distributions describing the event shapes are of interest for several reasons. Most of the variables are predicted to second order in QCD; some can also be resummed to all orders in α_s. By fitting the theoretical predictions to these distributions then the value of the strong coupling constant may be determined. By comparing with the direct predictions for the various Monte Carlo models, the validity of each model is tested.

In performing these determinations, the primary objective is to observe the running of the coupling with centre-of-mass energy; for this reason, the analyses at each energy point are designed, as far as possible, to be coherent with each other and to have correlated systematic errors. It is for this reason that the data at 133 GeV have been re-analysed with our new selections and procedures.

The event-shape variables studied thus far are as follows:

Thrust T: The thrust axis $\vec{n}_T$ is along the direction $\vec{n}$ which maximises the following quantity:

$$T = \left(\frac{\sum_i |\vec{p}_i \cdot \vec{n}|}{\sum_i |p_i|} \right) \quad . \tag{1}$$

The magnitude of the thrust vector is defined [14] as the value of the expression after maximisation.

Thrust major T_{major}: The thrust major vector, $\vec{T}_{T_{\mathrm{major}}}$, is defined in the same way as the thrust vector, but with the additional condition that $\vec{n}$ must lie in the plane perpendicular to $\vec{n}_T$.

Thrust minor T_{minor}: The thrust minor vector is again defined in the same way at the thrust vector but with the extra constraint that $\vec{n}_{T_{\mathrm{minor}}}$ which is perpendicular both to $\vec{n}_T$ and to $\vec{n}_{T_{\mathrm{major}}}$.

Oblateness O: The oblateness is defined by $O = T_{\mathrm{major}} - T_{\mathrm{minor}}$ [15].

Heavy Jet Mass M_h^2/s and Jet Mass Difference $(M_h^2 - M_l^2)/s$: A plane through the origin and perpendicular to $\vec{n}_T$ divides the event into two hemispheres, H_1 and H_2, from which one obtains corresponding hemisphere invariant masses. Labelling the heavier mass as M_h, the square of the mass is presented divided by s [19], as well as the mean of the square-root of this quantity. The former is to first order the same as $1 - T$, and is of use, for example, in comparison with lower-energy data when determining power-law hadronisation corrections [20]. The lighter of two masses is called M_l; mean values of the (quadratic) jet mass difference $(M_h^2 - M_l^2)/s$ are also reported.

Jet Broadening variables B_t and B_w: A measure of the broadening of particles in transverse momentum with respect to the thrust axis can be calculated for each hemisphere H_k using the relation

$$B_k = \left(\frac{\sum_{i\in} |\vec{p}_i \times \vec{n}_T|}{2 \sum_i |\vec{p}_i|} \right),$$

where i runs over all of the particles in the hemisphere under consideration. The two observables [21] are considered, defined by

$$B_t = B_1 + B_2 \quad \text{and} \quad B_w = \max(B_1, B_2)$$

where B_t is the total and B_w is the wide jet broadening.

Sphericity S and Aplanarity A: Both sphericity and aplanarity are based on the eigenvalues of the momentum tensor

$$S_{\alpha\beta} = \frac{\sum_i p_{i,\alpha} p_{i,\beta}}{\sum_i p_i^2} \quad , \quad \alpha, \beta = 1, 2, 3 \quad .$$

where α, β are the spatial co-ordinate labels. The three eigenvalues Q_j of $S_{\alpha\beta}$ are ordered such that $Q_1 < Q_2 < Q_3$. S [16] and A [17] are then defined by

$$S = \frac{3}{2}(Q_1 + Q_2) \quad \text{and} \quad A = \frac{3}{2} Q_1 \quad .$$

C-parameter C: The momentum tensor $S_{\alpha\beta}$ is linearised to become

$$M_{\alpha\beta} = \frac{\sum_i (p_{i,\alpha} p_{i,\beta})/|p_i|}{\sum_i |p_i|} \quad , \quad \alpha, \beta = 1, 2, 3 \quad .$$

The three eigenvalues λ_j of this tensor define C [18] with

$$C = 3(\lambda_1\lambda_2 + \lambda_2\lambda_3 + \lambda_3\lambda_1) \quad .$$

The observed data distributions for our selected events, after correcting for backgrounds and for detector effects by reweighting, are shown in Figs. 6 – 8 for the 133 GeV data, Figs. 9 – 11 for the 161 GeV data and Figs. 12 – 14 for the 172 GeV data. The data distributions are compared with those predicted by PYTHIA, HERWIG and ARIADNE version 4.08 [8], at hadron level.

In general, the agreement is good at all the energies considered in this paper. Exceptions are the aplanarity (A) and thrust-minor (T_{minor}) of the events at 161 GeV. Here the ALEPH data exceed the predictions at the higher end of the distributions. This is correlated with the excess of low-p_T particles observed at the same energy. In the 172 GeV data there is no real indication of an excess. OPAL has previously reported good agreement with the predictions at all energies in these distributions [22]. The mean

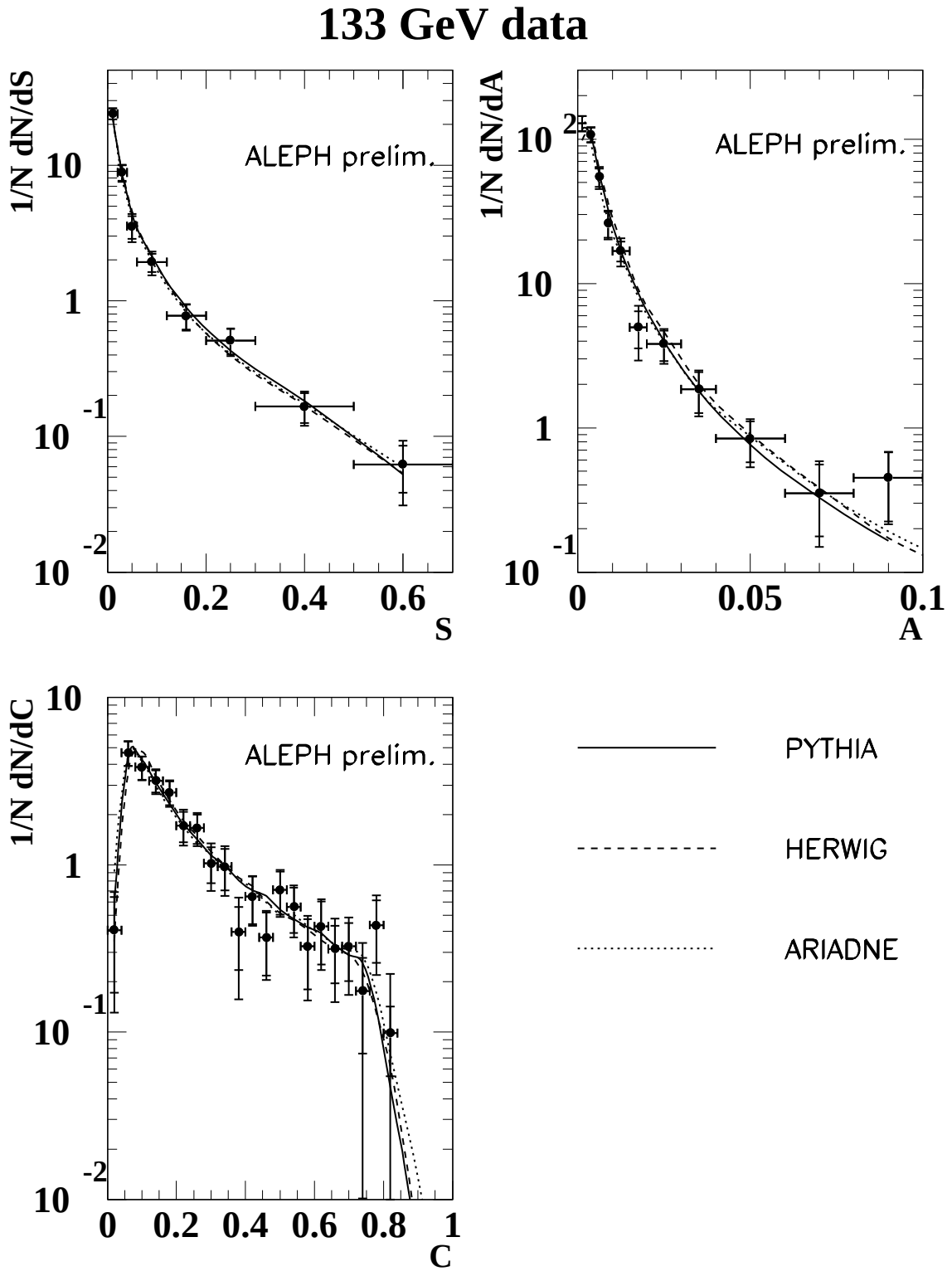

Figure 6: Distributions of Sphericity (S), Aplanarity (A) and C-parameter (C) at 133 GeV. Statistical and systematic errors are shown added in quadrature; the statistical error is also indicated.

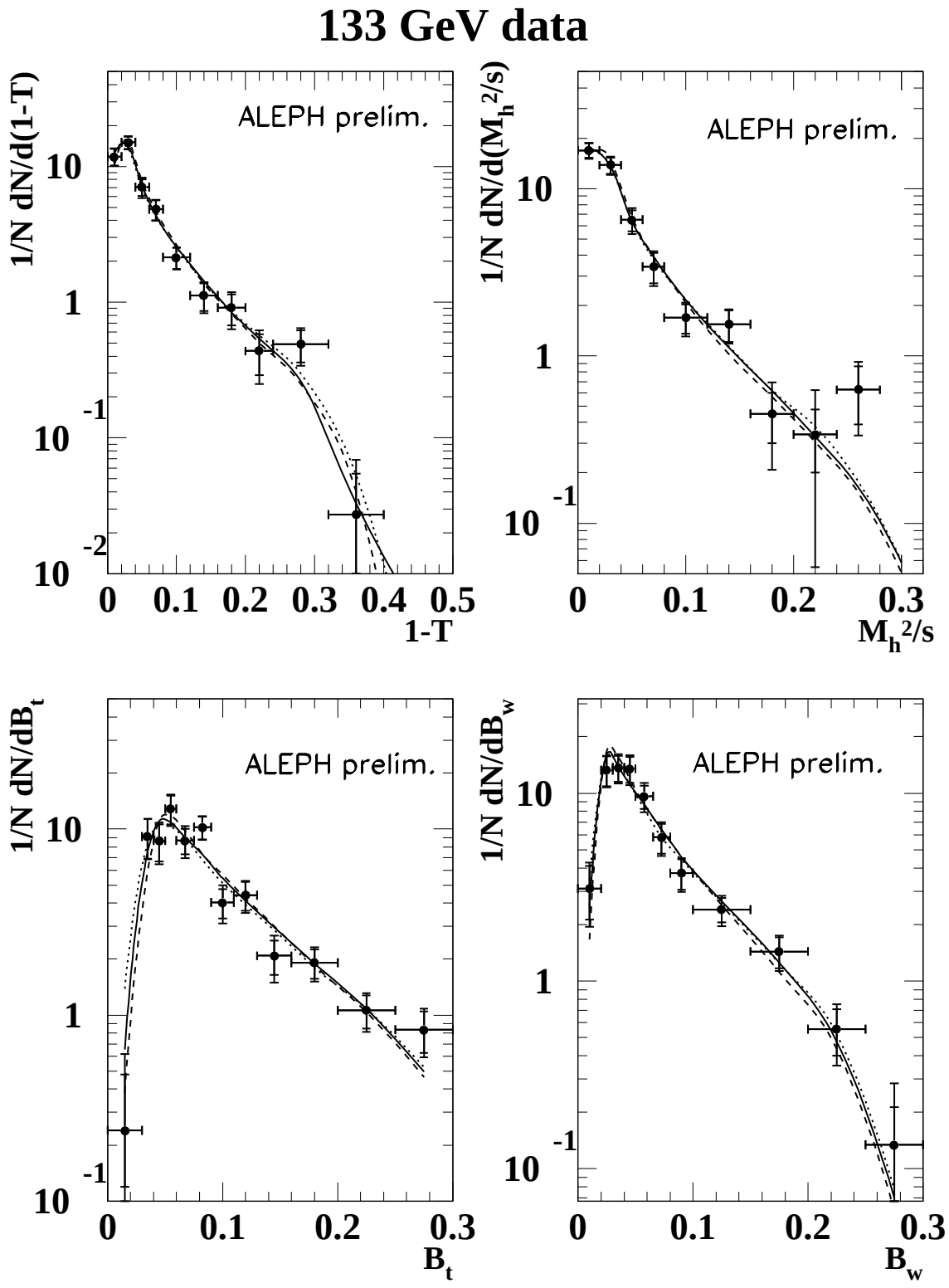

Figure 7: Distributions of 1-Thrust, scaled heavy-jet mass M_h^2/s and the wide-and total-jet broadenings (B_t and B_w) at 133 GeV. Statistical and systematic errors are shown added in quadrature; the statistical error is also indicated.

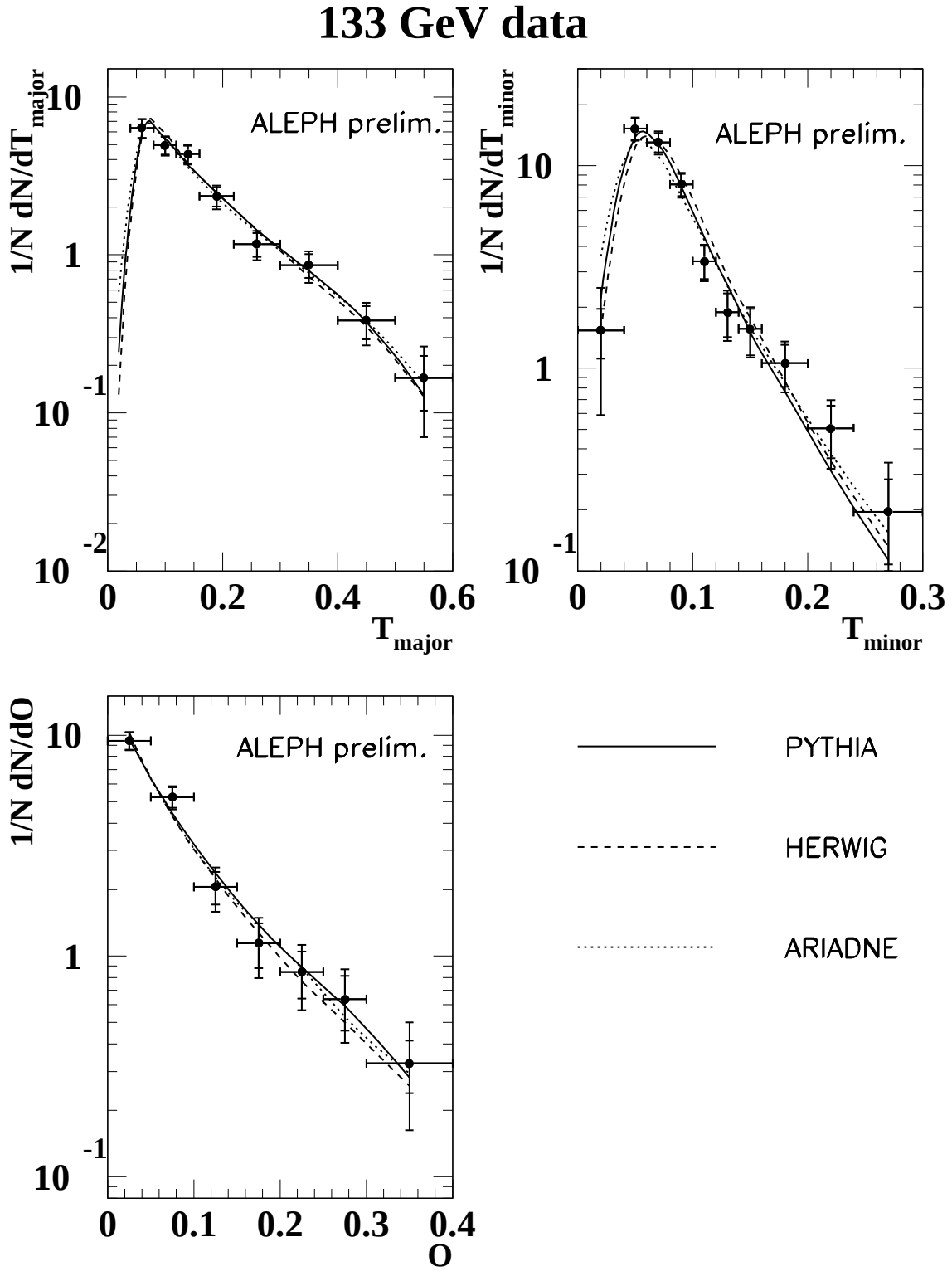

Figure 8: Distributions of $T_{\rm major}$, $T_{\rm minor}$, and Oblateness (O) at 133 GeV. Statistical and systematic errors are shown added in quadrature; the statistical error is also indicated.

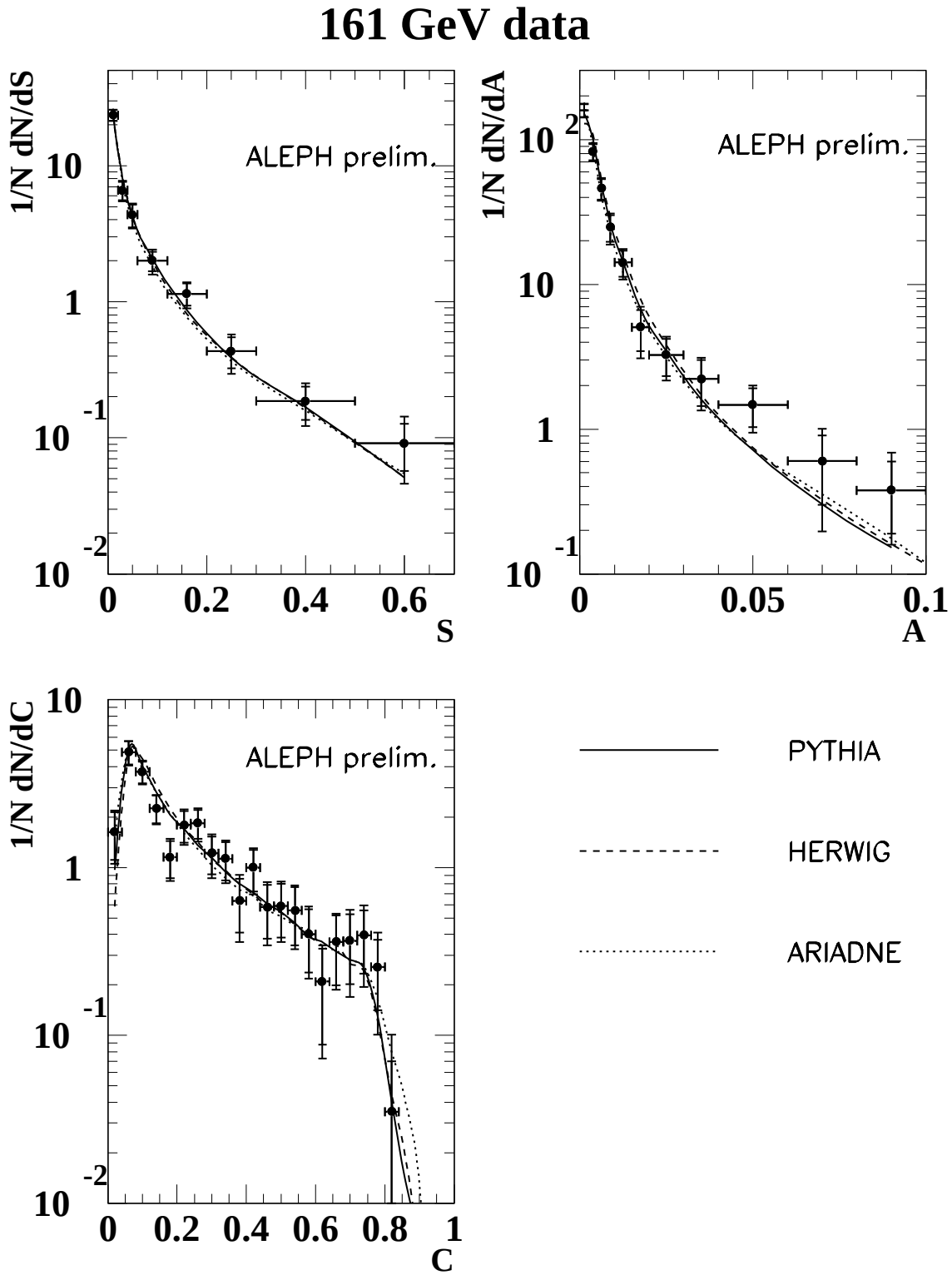

Figure 9: Distributions of Sphericity (S), Aplanarity (A) and C-parameter (C) at 161 GeV. Statistical and systematic errors are shown added in quadrature; the statistical error is also indicated.

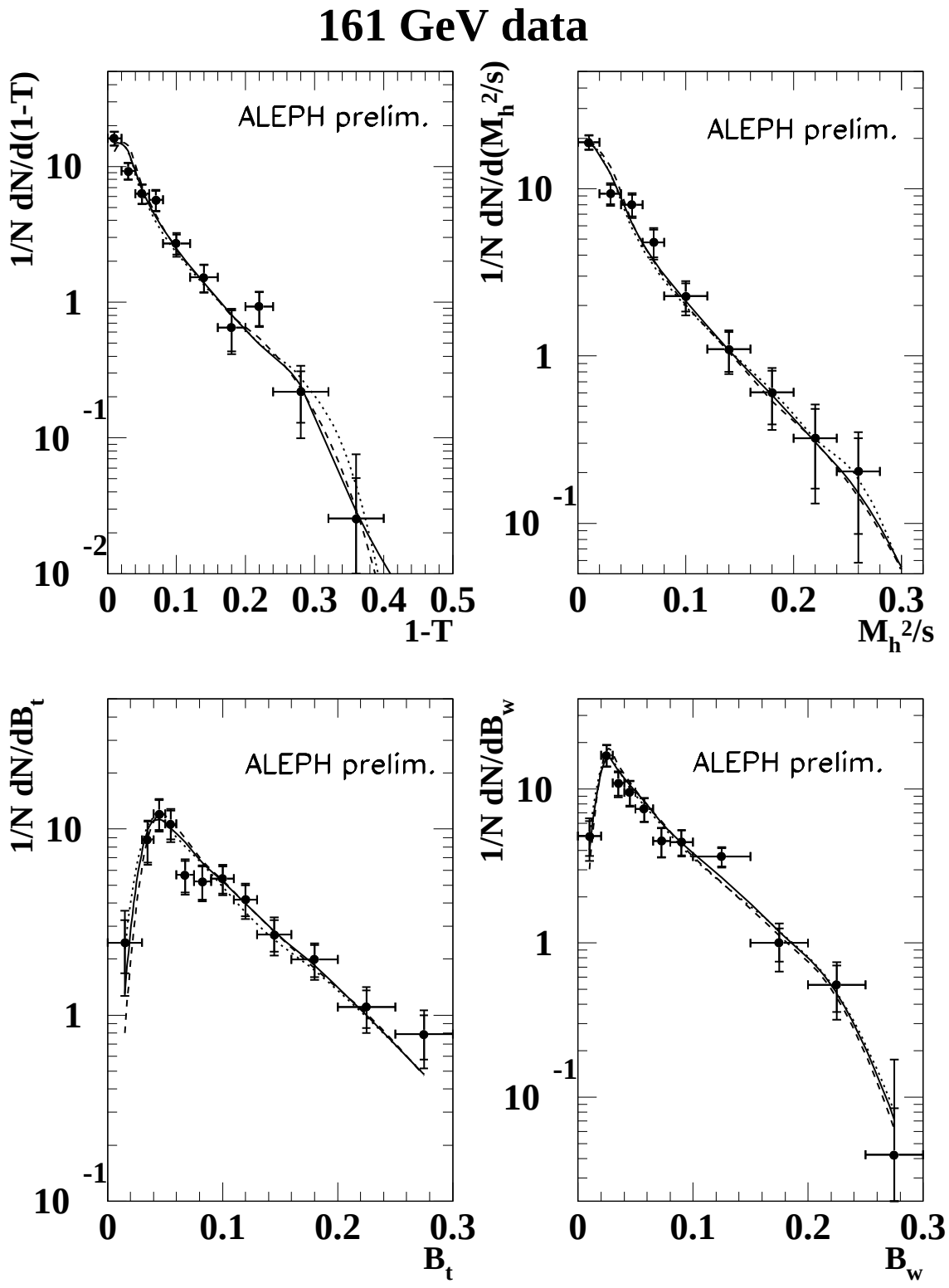

Figure 10: Distributions of 1-Thrust, scaled heavy-jet mass M_h^2/s and the wide-and total-jet broadenings (B_t and B_w) at 161 GeV. Statistical and systematic errors are shown added in quadrature; the statistical error is also indicated.

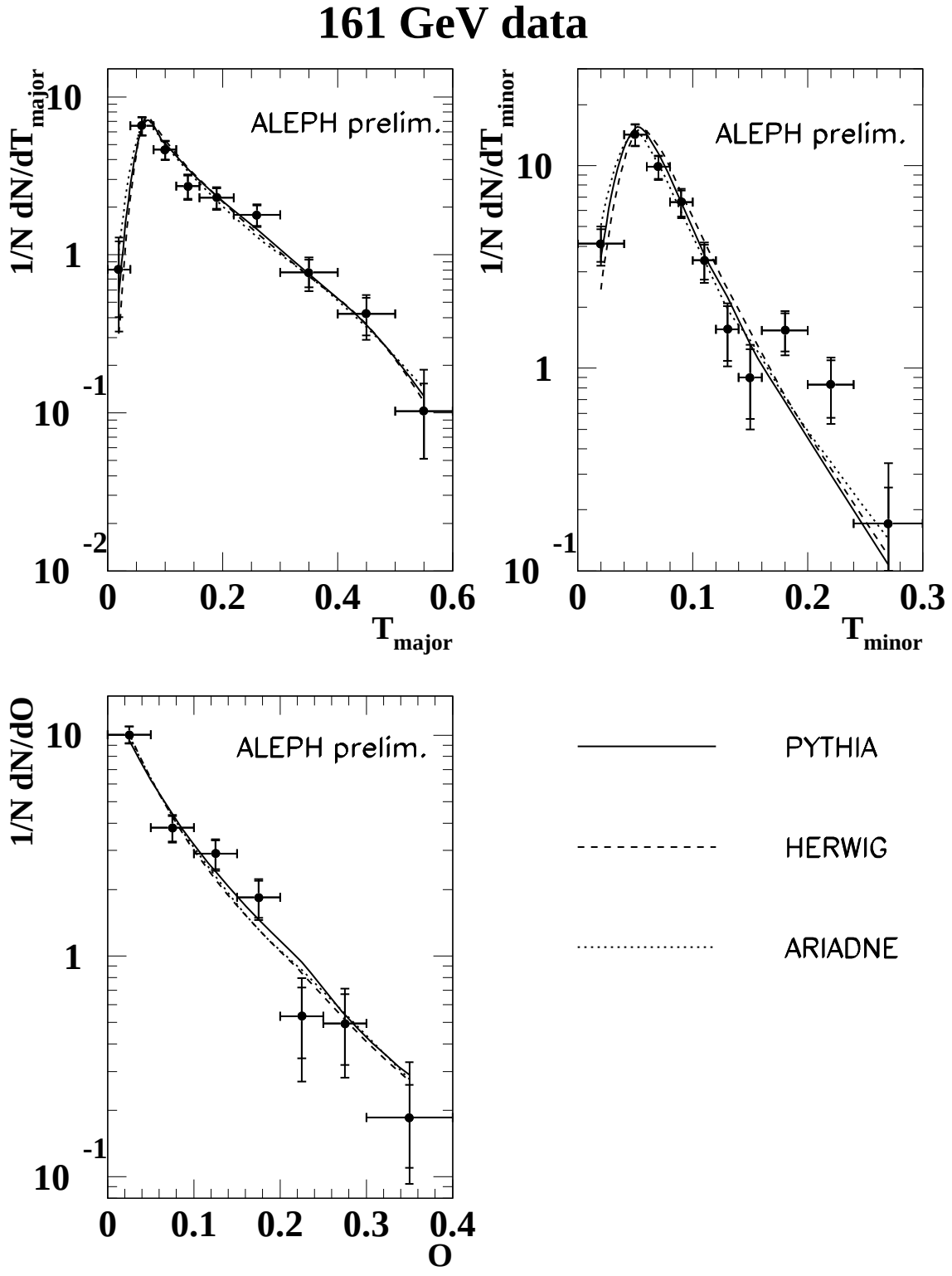

Figure 11: Distributions of $T_{\rm major}$, $T_{\rm minor}$, and Oblateness (O) at 161 GeV. Statistical and systematic errors are shown added in quadrature; the statistical error is also indicated.

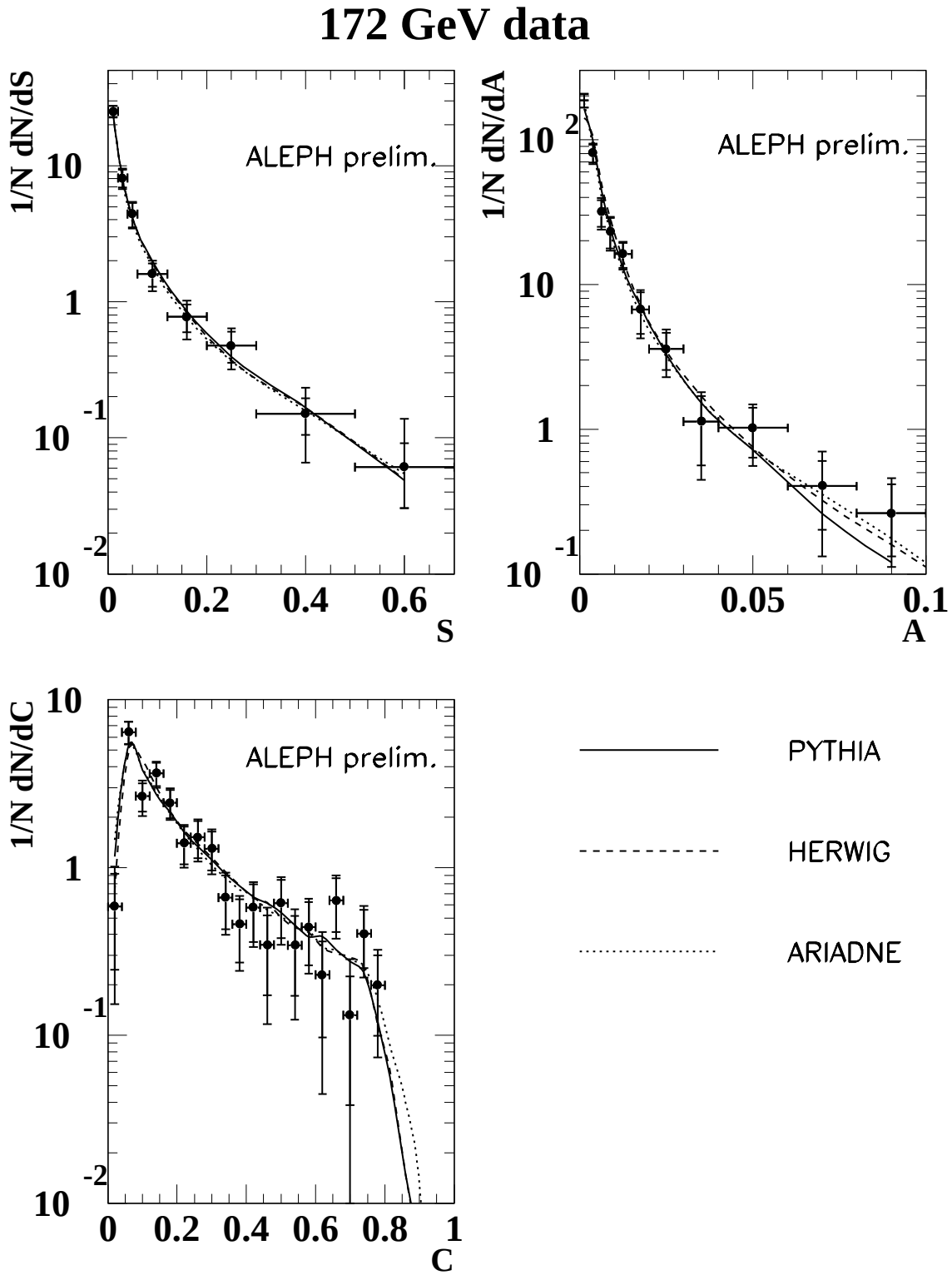

Figure 12: Distributions of Sphericity (S), Aplanarity (A) and C-parameter (C) at 172 GeV. Statistical and systematic errors are shown added in quadrature; the statistical error is also indicated.

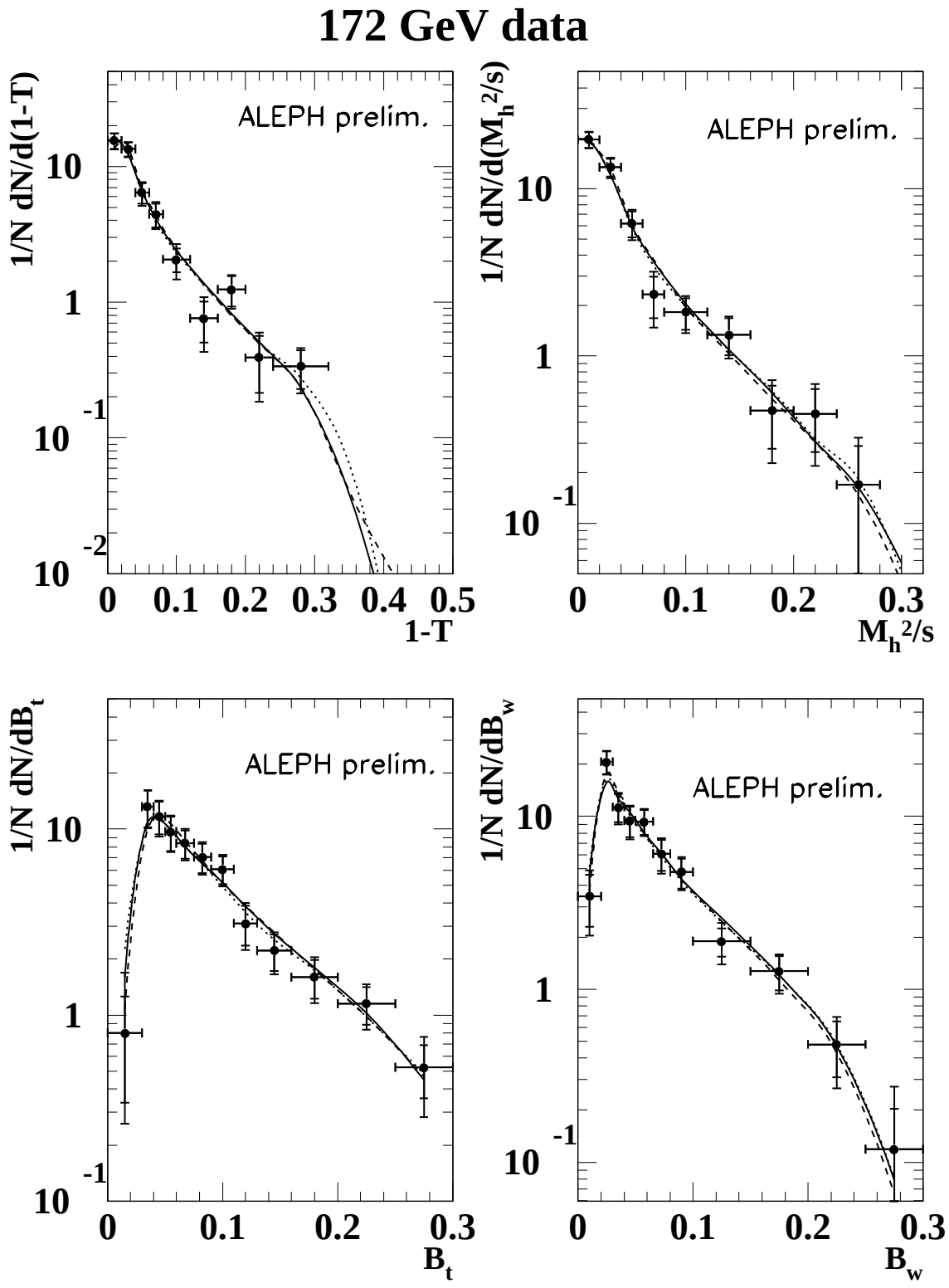

Figure 13: Distributions of 1-Thrust, scaled heavy-jet mass M_h^2/s and the wide-and total-jet broadenings (B_t and B_w) at 172 GeV. Statistical and systematic errors are shown added in quadrature; the statistical error is also indicated.

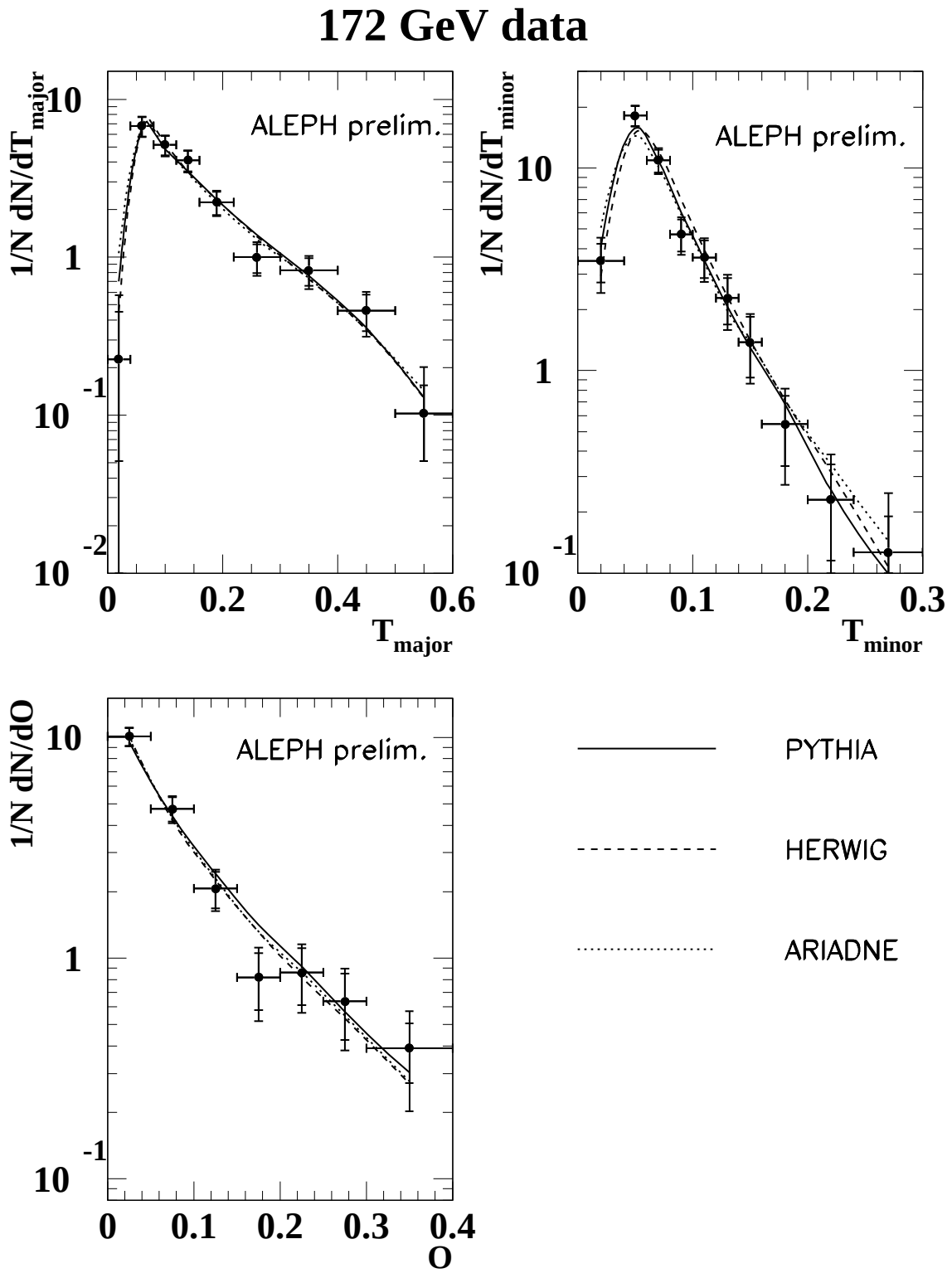

Figure 14: Distributions of $T_{\rm major}$, $T_{\rm minor}$, and Oblateness (O) at 172 GeV. Statistical and systematic errors are shown added in quadrature; the statistical error is also indicated.

	mean value	total error
$1-T$	$0.0627 \pm 0.0037 \pm 0.0042$	0.0056
T_{major}	$0.1663 \pm 0.0065 \pm 0.0075$	0.0099
T_{minor}	$0.0819 \pm 0.0025 \pm 0.0034$	0.0043
Oblateness	$0.0821 \pm 0.0046 \pm 0.0069$	0.0083
$M_h/\sqrt{s}$	$0.2003 \pm 0.0056 \pm 0.0069$	0.0088
M_h^2/s	$0.0515 \pm 0.0032 \pm 0.0028$	0.0042
$(M_h^2 - M_l^2)/s$	$0.0350 \pm 0.0028 \pm 0.0035$	0.0045
B_t	$0.1007 \pm 0.0036 \pm 0.0037$	0.0052
B_w	$0.0713 \pm 0.0030 \pm 0.0037$	0.0048
C	$0.2305 \pm 0.0109 \pm 0.0114$	0.0157
Sphericity	$0.0652 \pm 0.0059 \pm 0.0069$	0.0091
Aplanarity	$0.0090 \pm 0.0009 \pm 0.0013$	0.0016
Planarity	$0.0282 \pm 0.0027 \pm 0.0031$	0.0041

Table 3: The mean values of various event-shape variables at 133 GeV. The first error is statistical, the second systematic.

	mean value	total error
$1-T$	$0.0615 \pm 0.0037 \pm 0.0031$	0.0048
T_{major}	$0.1646 \pm 0.0069 \pm 0.0058$	0.0090
T_{minor}	$0.0805 \pm 0.0030 \pm 0.0024$	0.0039
Oblateness	$0.0791 \pm 0.0044 \pm 0.0040$	0.0060
$M_h/\sqrt{s}$	$0.1986 \pm 0.0057 \pm 0.0045$	0.0073
M_h^2/s	$0.0487 \pm 0.0029 \pm 0.0020$	0.0035
$(M_h^2 - M_l^2)/s$	$0.0330 \pm 0.0026 \pm 0.0013$	0.0029
B_t	$0.0983 \pm 0.0039 \pm 0.0039$	0.0055
B_w	$0.0697 \pm 0.0030 \pm 0.0022$	0.0037
C	$0.2305 \pm 0.0115 \pm 0.0088$	0.0145
Sphericity	$0.0730 \pm 0.0068 \pm 0.0055$	0.0087
Planarity	$0.0295 \pm 0.0029 \pm 0.0023$	0.0037
Aplanarity	$0.0108 \pm 0.0013 \pm 0.0011$	0.0017

Table 4: The mean values of various event-shape variables at 161 GeV. The first error is statistical, the second systematic.

values corresponding to each of the above event-shape variables are given for each of the energies in Tables 3, 4 and 5 respectively. The means are calculated by reweighting each event to remove detector effects and backgrounds, and using the measured value of the variable for the event. This differs slightly from the procedure used in reference [1], where a corrected histogram was constructed and the weighted mean calculated from the bin contents and the value of the variable at the bin centres; this was found to give a biased

	mean value	total error
$1-T$	$0.0563 \pm 0.0038 \pm 0.0026$	0.0046
T_{major}	$0.1587 \pm 0.0071 \pm 0.0048$	0.0086
T_{minor}	$0.0725 \pm 0.0025 \pm 0.0021$	0.0033
Oblateness	$0.0815 \pm 0.0053 \pm 0.0034$	0.0063
$M_h/\sqrt{s}$	$0.1903 \pm 0.0061 \pm 0.0048$	0.0078
M_h^2/s	$0.0454 \pm 0.0031 \pm 0.0029$	0.0043
$(M_h^2 - M_l^2)/s$	$0.0324 \pm 0.0029 \pm 0.0026$	0.0039
B_t	$0.0937 \pm 0.0039 \pm 0.0028$	0.0048
B_w	$0.0674 \pm 0.0032 \pm 0.0022$	0.0039
C	$0.2147 \pm 0.0118 \pm 0.0092$	0.0149
Sphericity	$0.0621 \pm 0.0065 \pm 0.0055$	0.0085
Planarity	$0.0282 \pm 0.0032 \pm 0.0025$	0.0040
Aplanarity	$0.0072 \pm 0.0008 \pm 0.0006$	0.0010

Table 5: The mean values of various event-shape variables at 172 GeV. The first error is statistical, the second systematic.

estimate of the true mean. The systematic errors have been discussed in Section 2.

5 Determination of jet rates

Jet rates are defined by means of the Durham clustering algorithm [2] in the following way. For each pair of particles i and j in an event one computes

$$y_{ij} = \frac{2\min(E_i^2, E_j^2)(1-\cos\theta_{ij})}{E_{vis}^2} \,. \tag{2}$$

The pair of particles with the smallest value of y_{ij} is replaced by a pseudo-particle (cluster). The four-momentum of the cluster is taken to be the sum of the four momenta of particles i and j, $p^\mu = p_i^\mu + p_j^\mu$ ("E" recombination scheme). The clustering procedure is repeated until all y_{ij} values exceed a given threshold y_{cut}. The number of clusters remaining at this point is defined to be the number of jets. Alternatively, one can continue the algorithm until exactly three clusters remain. The smallest value of y_{ij} in this configuration is defined as y_3. In this way one obtains a single number for each event, whose distribution is sensitive to the probability of hard gluon radiation leading to a three-jet topology. This can then be used to determine α_s (Section 6).

The n-jet rates were measured for $n = 2, 3, 4, 5$ and $n \geq 6$. Detector correction factors were applied in the same manner as for the event-shape distributions, but here for each value of the jet resolution parameter y_{cut}. Results are shown in Fig. 15 along with the predictions of PYTHIA and HERWIG.

A large excess compared to Monte Carlo expectations in the four, five and six-jet rates is seen at 161 GeV, but not at 133 or 172 GeV. It should be noted, however, that

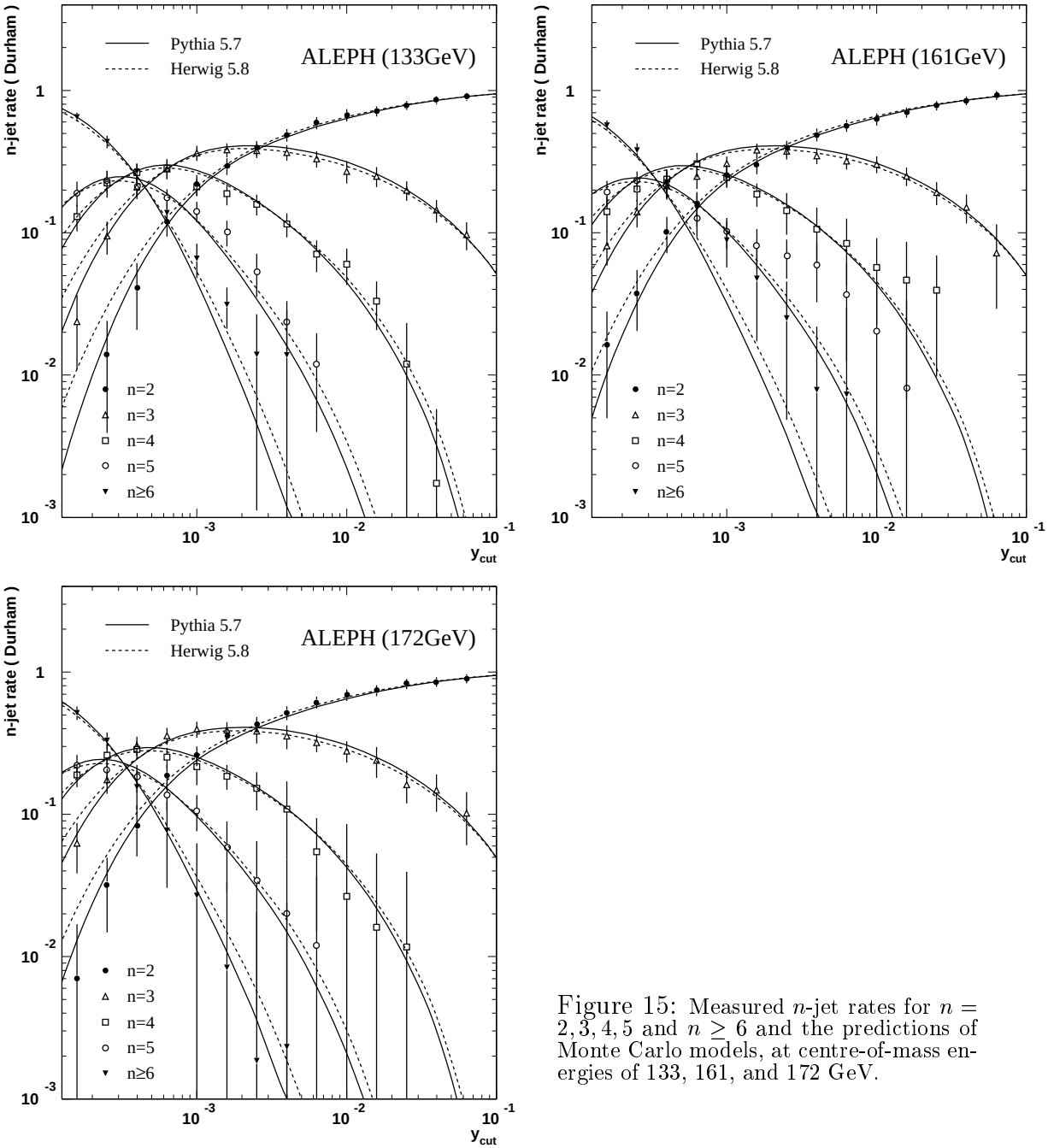

Figure 15: Measured n-jet rates for $n = 2, 3, 4, 5$ and $n \geq 6$ and the predictions of Monte Carlo models, at centre-of-mass energies of 133, 161, and 172 GeV.

neighbouring data points are highly correlated. No significant evidence was found that could related the excess events to an improper modeling of ISR or WW events, or to a detector effect. The fact that no excess is seen at 133 and 172 GeV clearly restricts the range of explanations; the most likely explanation is a large statistical fluctuation in the 161 GeV data.

6 Determination of α_s

QCD predicts that the value of the strong coupling constant, α_s, should fall by approximately 9% between 91 and 172 GeV. Unfortunately, as we have very few events at high energy with which to measure α_s, the uncertainties associated with the measurements approach the expected change in values. However, if the analysis is constructed such that the systematic uncertainties are highly correlated between the measurements at the different energies, an observation of the running of the coupling is still possible. In order to optimise the analysis with respect to the running of the coupling, a common fitted variable and fit range are selected for the determinations. This has entailed a change in the analysis since our published values for the 133 GeV data, and hence those data have been re-analysed.

The determination of α_s is very similar to that performed in reference [1]. The fitted variable is $-\ln y_3$, where y_3 is the value of cut on scaled invariant mass at which the event changes from being clustered into three jets to being clustered into two jets; the Durham clustering algorithm is chosen, with the 'E' scheme chosen for the combination of four-momenta. This variable has the virtue of requiring small corrections to translate from parton- to hadron-level values [23]. The perturbative QCD prediction is based on the $O(\alpha_s^2)$ matrix element [24], improved by including resummed leading and next-to-leading logarithmic terms [25, 26]. Matching the fixed order and resummed parts is done by means of the R and $\ln R$ matching schemes [27]. For the final value an average of the two results was taken using $\mu^2 = s$ for the renormalisation scale.

The analysis was carried out very much as in our previous paper [1]. Two differences should be noted: The fit was confined to the six bins in the range $1.2 \leq -\ln y_3 \leq 6$; this was for compatibility between the energy points and to reduce the hadronisation uncertainties. In addition, the statistical fit procedure no longer uses a covariance matrix based on a multinomial distribution, but rather is based on a simple least squares fit using diagonal errors only. This reduces the sensitivity to theoretical uncertainties in the distribution outside the fit range. Fit results are shown in Figs. 16.

The experimental systematic errors were determined by variation of cuts, as described for the other event-shape distributions (Section 4). The hadronisation corrections used in the analysis were taken from ARIADNE, which gave the best description of the data at 91.2 GeV. The corresponding uncertainty is estimated by using HERWIG or PYTHIA instead, and taking the largest change (which came from HERWIG) as the error. To estimate the uncertainty due missing higher orders in the perturbative prediction, the two matching schemes R and $\ln R$ were used, and the renormalisation scale μ was varied in the range $-1 \leq \ln \mu^2/s \leq 1$. The largest difference compared to the standard result under these changes is taken as the theoretical error. This component of the error should be highly correlated between the energy points. The hadronisation errors should also be correlated, though decreasing with increasing energy, and are already small. There is also a large degree of correlation between the experimental uncertainties. These are not fully correlated, however, since backgrounds and the effects of various cuts change somewhat with energy.

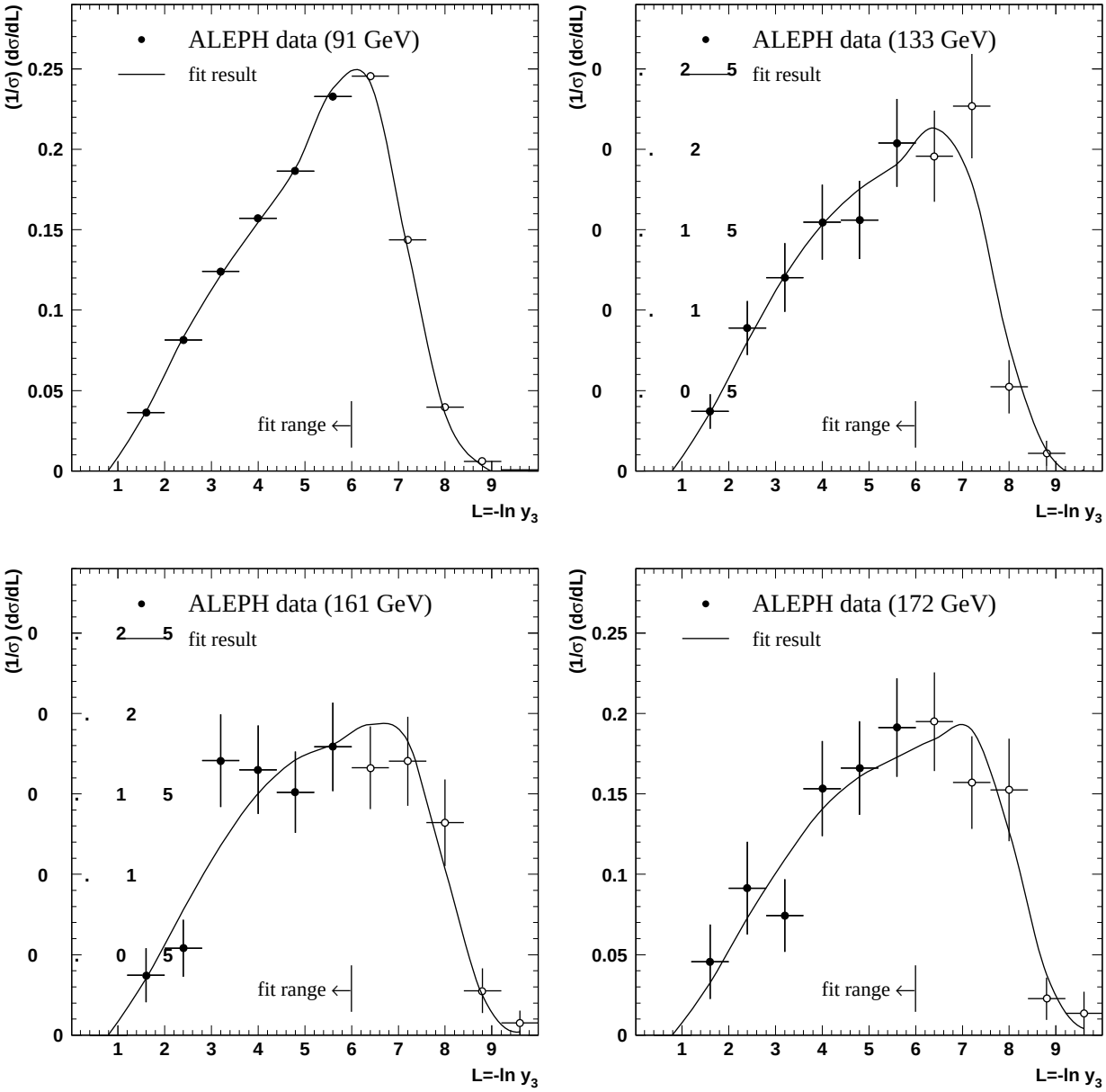

Figure 16: The measured distributions of $-\ln y_3$ at 91.2, 133, 161 and 172 GeV with the fitted QCD predictions. The solid points are used in the fit.

The resulting α_s measurements are given in Table 6 for the various energies, and also for some 110000 events from the 1992 running period at a centre-of-mass energy of 91.2 GeV. The results are also shown in graphical form in Fig. 17, along with the fitted two-loop prediction of QCD. While the evidence of running is not compelling, it should be remembered that much of the uncertainties between the points are highly correlated, though in a way not trivial to quantify.

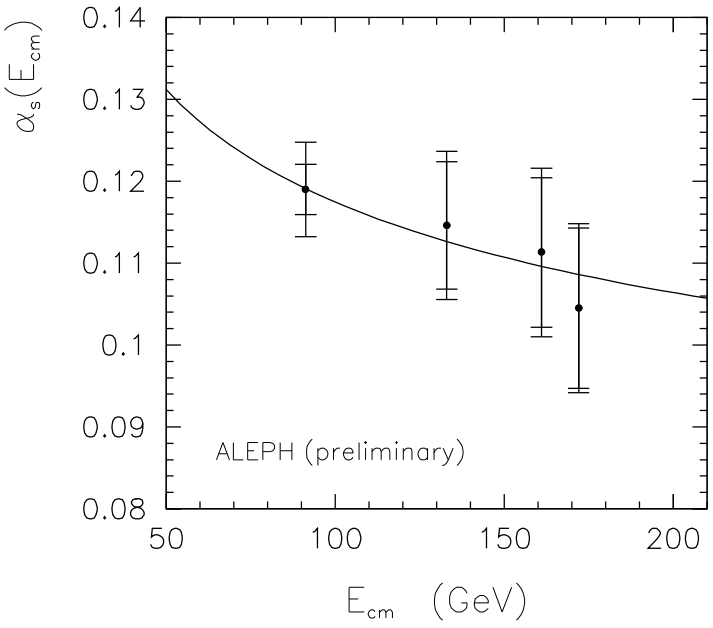

Figure 17: The strong coupling constant α_s measured at 91.2, 133, 161 and 172 GeV using the distribution of the variable $-\ln y_3$. The outer error bars indicate the total error. The inner error bars exclude the theoretical error, which is expected to be highly correlated between the measurements.

$\sqrt{s}$	α_s	stat.	syst.	hadron.	theory
91.2	0.1190	$\pm$0.0007	$\pm$0.0023	$\pm$0.0019	0.0049
133	0.1146	$\pm$0.0069	$\pm$0.0033	$\pm$0.0014	0.0046
161	0.1113	$\pm$0.0080	$\pm$0.0042	$\pm$0.0014	0.0047
172	0.1045	$\pm$0.0085	$\pm$0.0046	$\pm$0.0014	0.0034

Table 6: Measured values for the α_s at the various centre-of-mass energies. The value at 91.2 GeV is from the same analysis procedure as for the higher energy points applied to a subset of the available data, and is included in order to optimise the investigation of the running of the coupling.

7 Conclusions

Preliminary results are presented for analyses of hadronic events recorded by ALEPH at centre-of-mass energies of 161 and 172 GeV. In addition, previously published measurements at 133 GeV are updated and extended. Overall, the measurements show reasonable agreement with the predictions of Monte Carlo models and analytic QCD predictions. At 161 GeV, however, a significant excess in multijet events is observed. The energy evolution of derived quantities such as the mean multiplicity of charged particles $N_{\rm ch}$, the peak position ξ^* of the inclusive charged particle distribution of $\xi = -\ln x_p$, and the strong coupling constant α_s has been investigated. For α_s, the energy evolution from $E_{\rm cm} = 91.2$ to 172 GeV is in good agreement with QCD expectations, but the statistical errors at the higher energy points are large. A more statistically significant investigation of the running of α_s will become possible when additional high energy data becomes available.

Acknowledgements

We wish to thank our colleagues from the accelerator divisions for the successful operation of LEP. It is also a pleasure to thank the technical personnel of the collaborating institutions for their support in constructing and maintaining the ALEPH experiment. Those of the collaboration not from member states thank CERN for its hospitality.

References

[1] D. Buskulic et al., ALEPH Collab., Z. Phys. C73 (1997) 409.

[2] S. Catani et al., Phys. Lett. B269 (1991) 432;
W.J. Stirling et al., Proceedings of the Durham Workshop, J. Phys. G: Nucl. Part. Phys. 17 (1991) 1567;
N. Brown and W.J. Stirling, Phys. Lett. B252 (1990) 657;
S. Bethke et al., Nucl. Phys. B370 (1992) 310.

[3] D. Decamp et al., ALEPH Collab., Nucl. Instr. Meth. A 294 (1990) 121.

[4] D. Decamp et al., ALEPH Collab., Phys. Rep. 216 (1992) 253; D. Buskulic et al., ALEPH Collab., Nucl. Instr. Meth. A360 (1995) 481.

[5] T. Sjöstrand, Computer Physics Commun. 82 (1994) 74.

[6] M. Skrzypek, S. Jadach, W. Placzek and Z. Was, Computer Physics Commun. 94 (1996) 216.

[7] G. Marchesini, B.R. Webber, G. Abbiendi, I.G. Knowles, M.H. Seymour, and L. Stanco, Comp. Phys. Comm. 67 (1992) 465.

[8] L. Lönnblad, Computer Physics Commun. 71 (1992) 15.

[9] R. Barate et al., ALEPH Collab., *Studies of Quantum Chromodynamics with the ALEPH Detector*, CERN / PPE 96-186, to appear in Physics Reports.

[10] Y.K. Li et al., AMY Collab., Phys. Rev. D41 (1990) 2675;
H.W. Zheng et al., AMY Collab., Phys. Rev. D42 (1990) 737;
W. Braunschweig et al., TASSO Collab., Z. Phys. C45 (1989) 193;
W. Bartel et al., JADE Collab., Z. Phys. C20 (1983) 187;
M. Derrick et al., HRS Collab., Phys. Rev. D34 (1986) 3304;
P. Abreu et al., DELPHI Collab., Z. Phys. C50 (1991) 185;
P. Abreu et al., DELPHI Collab., Phys. Lett. B372 (1996) 172;
B. Adeva et al., L3 Collab., Z. Phys. C55 (1992) 39;
M. Acciarri et al., L3 Collab., Phys. Lett. B371 (1996) 173;
M. Acciarri et al., L3 Collab., CERN-PPE/97-42;
P.D. Acton et al., OPAL Collab., Z. Phys. C53 (1992) 539;
G. Alexander et al. OPAL Collab., Z. Phys. C72 (1996) 191;
K. Ackerstaff et al., OPAL Collab., CERN-PPE/97-015, accepted by Z. Phys. C.

[11] C.P. Fong and B.R. Webber, Phys. Lett. B229 (1989) 289.

[12] Yu.L. Dokshitzer, V.A. Khoze, A.H. Mueller and S.I. Troyan, *Basics of Perturbative QCD*, Editions Frontières, Gif-sur-Yvette, 1991.

[13] W. Braunschweig et al., TASSO Collab., Z. Phys. C47 (1990) 187.

[14] S. Brandt et al., Phys. Lett. 12 (1964) 57;
E. Farhi, Phys. Rev. Lett. 39 (1977) 1587.

[15] D.P. Barber et al., MARK J Collab., Phys. Rev. Lett. 43 (1979) 830.

[16] J.D. Bjorken and S.J. Brodsky, Phys. Rev. D1 (1970) 1416;
G. Hanson et al., SLAC-LBL Collab., Phys. Rev. Lett. 35 (1975) 1609.

[17] S.L. Wu and G. Zobernig, Z. Phys. C2 (1979) 107.

[18] G. Parisi, Phys. Lett. B74 (1978) 65;
J.F. Donoghue, F.E. Low, and S.Y. Pi, Phys. Rev. D20 (1979) 2759.

[19] T. Chandramohan and L. Clavelli, Nucl. Phys. B184 (1981) 365;
L. Clavelli and D. Wyler, Phys. Lett. B103 (1981) 383.

[20] The ALEPH Collab., *Power Law Corrections to Hadronic Event Shape Variables in* e^+e^- *Annihilation*, contribution to EPS-HEP97, Jerusalem, 19–26 August 1997, reference number 610.

[21] S. Catani, G. Turnock and B.R. Webber, Phys. Lett. B295 (1992) 269.

[22] G. Alexander et al., OPAL Collab., Z. Phys. C72 (1997) 191;
K. Ackerstaff et al., OPAL Collab., CERN-PPE/97-015, accepted by Z. Phys. C.

[23] Yu. L. Dokshitzer, G. Marchesini and B. R. Webber: CERN-TH/95-281, 1995.

[24] R.K. Ellis, D.A. Ross and A.E. Terrano, Nuclear Physics B178 (1981) 421.

[25] Proceedings of the Durham Workshop, W.J. Stirling, J. Phys. G: Nucl. Part. Phys. 17 (1991) 1567;
N. Brown and W.J. Stirling, Phys. Lett. B252 (1990) 657;
S. Bethke, Z. Kunszt, D.E. Soper and W.J. Stirling, Nucl. Phys. B370 (1992) 310.

[26] G. Dissertori and M. Schmelling, Phys. Lett. B361 (1995) 167.

[27] D. Decamp et al., ALEPH Collab., Phys. Lett. B284 (1992) 163.